

Contents lists available at SciVerse ScienceDirect

## Journal of Alloys and Compounds

journal homepage: www.elsevier.com/locate/jalcom



# Low Fe-doped Bi<sub>2</sub>O<sub>3</sub> photocatalyst with long wavelength response: Crystalline transition and mechanisms by first-principles calculation

Yunrong Dai, Lifeng Yin\*

State Key Laboratory of Water Environment Simulation, School of Environment, Beijing Normal University, Beijing 100875, PR China

#### ARTICLE INFO

Article history:
Received 17 December 2012
Received in revised form 7 February 2013
Accepted 14 February 2013
Available online 26 February 2013

Keywords: Photocatalyst Visible light Crystalline transition First-principles calculation

#### ABSTRACT

The low Fe-doped  $Bi_2O_3$  with different crystalline phases was synthesized by a solvothermal method. With the increase of annealing temperature, the crystalline phase of the low Fe-doped  $Bi_2O_3$  was transformed from  $Bi_2O_2CO_3$  to monoclinic  $\alpha$ - $Bi_2O_3$  and cubic  $Bi_{25}FeO_{40}$ . Among them, the mixture of  $\alpha$ - $Bi_2O_3$  and  $Bi_{25}FeO_{40}$  (annealed at  $600\,^{\circ}C$ ) showed the highest photocatalytic activity for decomposing pentachlorophenol (PCP) under visible light irradiation (99.2% removal rate). Both theoretical calculations and experimental results support that Fe-doping brings about the hybridization of the energy levels and the modification of electron structure, which is responsible for extending the photoabsorptivity to the visible light region (<623 nm) and strengthening the photocatalytic activity of Fe-doped  $Bi_2O_3$ .

© 2013 Elsevier B.V. All rights reserved.

#### 1. Introduction

Semiconductor photocatalysis has attracted increasing attention for solar energy harvest (dye sensitized solar cells and photocatalytic water splitting) and environmental remediation (photocatalytic decomposition of pollutants in water and soil) [1]. One obstacle to its effective use is the inadequate absorption for visible light in sunlight [2]. Therefore, many visible-light-driven photocatalysts have been developed for the practical applications. Among them, Bi-based oxides were testified to be efficient photocatalysts for the degradation of environmental pollutants. The typical Bi-based oxides, including  $Bi_2O_3$  [3],  $BiVO_4$  [4],  $Bi_2WO_6$  [5],  $Bi_2MOO_6$  [6], and  $BiTa_{1-x}Nb_xO_4$  [7], are potential candidates for removing pollutants including 4-chlorophenol, rhodamin B, ibu-profen and naproxen from contaminated aqueous environment.

Currently, it has been found that bismuth iron oxides are excellent semiconductor photocatalysts and perform better than nano-TiO<sub>2</sub> (P25, Degussa) [8,9]. It has been evidenced that BiFeO<sub>3</sub> is a visible light driven photocatalyst with narrow band gap ( $\sim$ 2.1 eV) [9]. However, most researches focused on the synthesis and photocatalytic activity of pure BiFeO<sub>3</sub> with equal mole fraction of Bi and Fe. Few involved in the crystalline transformation and photoabsorptivity of low Fe-doped Bi<sub>2</sub>O<sub>3</sub>. Recently, doping photocatalyst with metal atom has been a popular method to improve the performance of a photocatalyst [10–12]. The heterogeneous synthesis might bring about the new doping levels in the band

gap of the semiconductor photocatalyst, resulting in wider light response [13].

In this study, we explored the effect of Fe-doping on the photoabsorptivity and photocatalytic activity of  $Bi_2O_3$ . The various crystalline phases, which were closely related to the photocatalytic activity, were obtained under the different annealing temperatures. According to the experimental results, the annealing temperature was optimized for the best photocatalytic activity. Simultaneously, the strengthened photoabsorptivity was attributed to the reconstruction of the electron structure of  $Bi_2O_3$  induced by Fe-doping.

#### 2. Experimental

#### 2.1. Synthesis of low Fe-doped Bi<sub>2</sub>O<sub>3</sub>

First, 2.4 mmol of Bi(NO $_3$ ) $_3$ ·SH $_2$ O was dissolved in 10 mL of absolute acetic acid with vigorous stirring, and then 0.1 mmol Fe(NO $_3$ ) $_3$  was added into this solution to get a pink suspensions. The solution was further stirred overnight and transferred into a Teflon lined autoclave (100 mL), which was sealed and kept at 140 °C. After 36 h, the resulting gray product was filtered, washed with distilled water, and dried at 120 °C for 2 h. To study the change of the crystalline phase, the obtained samples were further annealed at 200 °C, 300 °C, 400 °C, 500 °C, and 600 °C for 5 h, and the products were labeled as BFO200–BFO600, respectively.

#### 2.2. Characterization

All samples were characterized by X-ray powder diffraction (XRD). The XRD measurements were conducted on an X' Pert PRO MPD diffractometer (USA) with Cu K $\alpha$  radiation ( $\lambda$  = 1.518 A). The operating voltage and current were kept at 35 kV and 40 mA, respectively. A scan rate of  $5^{\circ}$  min<sup>-1</sup> was applied to record the patterns in the  $2\theta$  range  $10-80^{\circ}$ . The morphology and microstructure were characterized with a scanning electron microscope (SEM, S4800, Hitachi, Japan). Binding

<sup>\*</sup> Corresponding author. Tel./fax: +86 10 58807612. E-mail address: lfyin@bnu.edu.cn (L. Yin).

energies were measured by X-ray photoelectron spectroscopy (XPS) with a PHI 5600 XPS instrument employing pressed powder pellets contacted by silver lacquer with an aluminum foil. All XPS spectra were referenced to the C1s peak of adventious hydrocarbon contamination located at 284.8 eV. Fitting of the XPS data was accomplished using XPS Peak software. Special surface area was measured with a full-automatic ASAP 2010 surface area and pore analyzer (Micromeritics, USA) at liquid nitrogen temperature (–196 °C). The special surface areas were obtained using the Brunauer–Emmett–Teller method. UV–vis diffuse reflectance spectra (UV–vis DRS) of the samples were measured by using a spectrophotometer (Specord 200; Analytik Jena, Germany). BaSO<sub>4</sub> was used as the reference standard, and the spectrum was recorded in the range 200–800 nm.

#### 2.3. Photocatalytic decomposition

The photocatalytic decomposition was conducted under the irradiation by a Xenon lamp (CHF-XM-1000 W; Trusttech, China) with a cut-off filter at 420 nm (SCF-S50-42L; Sigma Koki, Japan). About 0.05 g photocatalyst was scattered in 100 mL of 10 mg L $^{-1}$  pentachlorophenol (PCP) solution at a constant-temperature of 25 °C. Before the irradiation, the suspensions were kept in dark for 30 min to reach the adsorption–desorption equilibrium. Then the suspensions were transferred to a 250 mL beaker as the photoreactor. The beaker was placed 5 cm below the Xenon lamp and under constant air-equilibrated conditions before and during the irradiation. The PCP solution was sampled each 10 min and analyzed by recording PCP concentration with high-performance liquid chromatography (HPLC; Waters 600, USA).

#### 3. Band structure calculation

The band structure and the density of states (DOSs) of Fe-doped  $Bi_2O_3$  were calculated using the ABINIT program package. The ABINIT calculation included the plane-wave pseudo-potential total energy method based on the density functional theory (DFT). The geometry optimization and the local density approximation (LDA) were applied. The unit cell selected for calculation was Fedoped  $Bi_2O_3$  (a Fe atom replaced one of 24 Bi atoms in a  $2 \times 2 \times 1$   $Bi_2O_3$  supercell). The kinetic energy cutoff was 300 eV.

#### 4. Results and discussion

#### 4.1. Surface analysis

The morphology and microstructure of low Fe-doped  ${\rm Bi_2O_3}$  annealed under different temperatures were measured by the electron microscopy. The SEM images show the as-prepared product (Fig. 1a) and BFO200 (Fig. 1b) were clustered blocks with sizes of

20–50 nm. Annealed at 300–400 °C, the samples changed into smaller particles (Fig. 1c and d). The sample is a pile of regular blocks. The samples BFO500 and BFO600 were scattered with the similar particle sizes with those obtained at 300–400 °C, but their morphologies became smoother, as shown in Fig. 1e and f. The morphology and microstructure of resulting samples were not similar with that of  $\alpha$ ,  $\beta$ , and  $\sigma$ -Bi<sub>2</sub>O<sub>3</sub>, as previous reported [14–16]. Probably, the Fe-doping decreased the surface energy of Bi<sub>2</sub>O<sub>3</sub> and regularized the morphologies of the particles [17].

The surface of a photocatalyst generally limits its photocatalysis. The BET surface area of BFO200–600 was 24.6, 31.7, 26.4, 30.9, and 27.8 m $^2$  g $^{-1}$ , respectively. Here, the sample obtained at 300 °C has the largest BET surface area, however, which is not much different from other samples. The results suggested that the photocatalytic activity of low Fe-doped Bi $_2$ O $_3$  depends on the absorptivity, energy band structure, and crystal form instead of their physical structures.

XPS analysis was carried out on BFO200–600. Here, the patterns of all samples were similar. Taking the BFO500 for example, the peaks for Fe 2p have been detected within 705–730 eV (Fig. 2). Especially, the XPS peaks of Fe  $2p_{3/2}$  and Fe  $2p_{1/2}$  are shown in Fig. 2 (inset). The binding energies of Fe  $2p_{3/2}$  and Fe  $2p_{1/2}$  are 711.5 ± 0.12 and 724.0 ± 0.05 eV, respectively, which has been reported with the values of 711.0 and 724.5 eV for Fe<sup>3+</sup> [18]. Therefore, in our case, it is Fe<sup>3+</sup> instead of Fe<sup>2+</sup> was introduced by low Fe-doping. Of the two peaks, Fe  $2p_{3/2}$  peak is stronger than Fe  $2p_{1/2}$  and the area of Fe  $2p_{3/2}$  peak is greater than that of Fe  $2p_{1/2}$  since the spin–orbit (j–j) coupling. The Fe  $2p_{3/2}$  peak has associated with satellite peaks. The satellite peak of Fe  $2p_{3/2}$  is located 3 eV higher than the Fe  $2p_{3/2}$  peak. The origin binging energy of Fe 2p suggests that the Fe<sup>3+</sup> was only bonded with O rather than other atoms.

#### 4.2. XRD analysis

Although the morphology of low Fe-doped  ${\rm Bi}_2{\rm O}_3$  did not change too much, their crystalline phases changed dramatically with the increase of the annealing temperatures. The XRD analysis of the samples showed that four main crystalline phases were created during the annealing (Fig. 3). The peaks of the BFO200 and BFO300 synthesized at lower annealing temperature can be

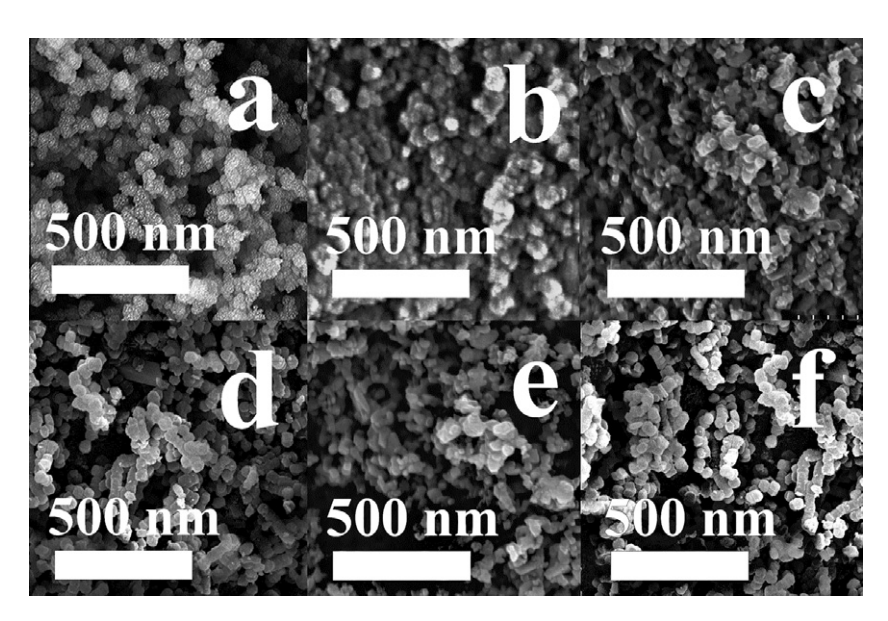


Fig. 1. The SEM (scanning electronic microscopic) images of as-prepared Fe-doped Bi<sub>2</sub>O<sub>3</sub> (a) and the samples anneal under 200 °C (b), 300 °C (c), 400 °C (d), 500 °C (e), and 600 °C (f).

### Download English Version:

# https://daneshyari.com/en/article/1614184

Download Persian Version:

https://daneshyari.com/article/1614184

<u>Daneshyari.com</u>